Supporting Information

Stacking of 2D electron gases in Ge probed at the atomic-level and its correlation to low temperature magnetotransport.

G. Scappucci,[1,2] W. M. Klesse,[1,2] A. R. Hamilton,[1] G. Capellini,[3] D. L. Jaeger,[4] M. R. Bischof,[4] R. F. Reidy,[4] B. P. Gorman,[5] and M. Y. Simmons[1,2]

[1]School of Physics, University of New South Wales, Sydney, NSW 2052, Australia.

[2]Australian Research Council Centre of Excellence for Quantum Computation and Communication Technology, University of New South Wales, Sydney, NSW 2052, Australia.

[3]Dipartimento di Fisica "E. Amaldi", Università di Roma Tre, Via della Vasca Navale 84, 00146 Roma, Italy.

[4]Department of Materials Science and Engineering, University of North Texas, Denton, Texas 76209, USA

[5]Department of Materials Science and Engineering, Colorado School of Mines, Golden, Colorado 80401, USA

Email: giordano.scappucci@unsw.edu.au

Supporting Information Contents

1. Atom Probe Tomography

As a first step to produce atom probe compatible specimens the as-received single and multilayer atomically abrupt P doped Ge thin film samples were coated with protective amorphous films of 25-60nm Cr / 20nm Pt using a broad ion beam sputter system (Gatan 682 Precision Etching and Coating system). The coated samples were then transferred to a focused ion beam (FIB)/scanning electron microscope (SEM) dual-beam system (FEI Nova 200 Nanolab, Hillsboro, OR) equipped with a Pt gas injection system deposition source and a micromanipulator (Omniprobe Autoprobe 200 nano-manipulator, Dallas, TX). Atom probe compatible needle specimens were prepared in the dual beam system using site specific lift-out techniques, then mounted to Si microtip posts (CAMECA Atom Probe Technology Center, Madison, WI) and finally annular milled. A final series of 5kV focused ion beam scans were applied to remove surface damage incurred during the FIB milling process and shape the end of the apex to an approximate hemispherical shape with an apex diameter of 65-80nm and at least 10nm of amorphous Cr film remaining on the tip apex.

Pulsed laser atom probe tomography was performed at the University of North Texas Center for Advanced Research and Technology (CART) using a Local Electrode Atom Probe (LEAP) 3000X HR (CAMECA Atom Probe Technology Center, Madison, WI) laser pulsed local electrode atom probe with a reflectron lens. Samples were analyzed at a base temperature of 30-50K in laser pulsed field evaporation mode using a pulsed laser with a wavelength of 532nm, pulse width of 10ps, applied at a pulse frequency of 160kHz, laser energy of 0.2-0.3nJ and an evaporation rate of 0.001-0.005 ions/pulse. The resulting tomographic atom probe data was analyzed using the atom probe reconstruction software, IVAS 3.6.1 (CAMECA Atom Probe Technology Center, Madison, WI). Reconstructions were correlated with Transmission Electron Microscopy and Secondary Ion Mass Spectrometry (SIMS) data.

The vertical and lateral distribution of the P dopants within the region of the delta doped layers, defined as the regions enclosed by 0.25% P isoconcentration surfaces, were analyzed within IVAS 3.6.2 to determine if the Atom Probe Tomography reconstructed P distributions can be considered to be distributed in an ordered or random fashion within the delta layer.[1] By inspection of the lateral P distribution present in the delta layers, as shown in Figure S1a, the dopants do not appear to cluster into well-defined particles or show ordering, but are qualitatively distributed homogeneously throughout the delta layer. Radial distribution function (RDF) analysis of

the delta doped regions (Figure S1b), indicates that P-P clustering is absent as indicated by the experimental P-P interaction which is centered about unity with respect to the error bars and when also compared to the P-P interaction due to a random distribution. The concentration frequency distribution of P within the delta layers, Figure S1c, does not deviate significantly from that of the binomial distribution and therefore does not indicate the presence of statistically significant P clusters. Comparison of the nearest neighbor distance between P ions present within the delta doped region and that expected for a random alloy as shown by the Binomial distribution curve (Figure S1d), indicates that distances between P nearest neighbors correspond to those expected of a random alloy. Collectively, this qualitative and quantitative analysis shows that the position of P atoms is distributed randomly within the plane of the δ-layers.

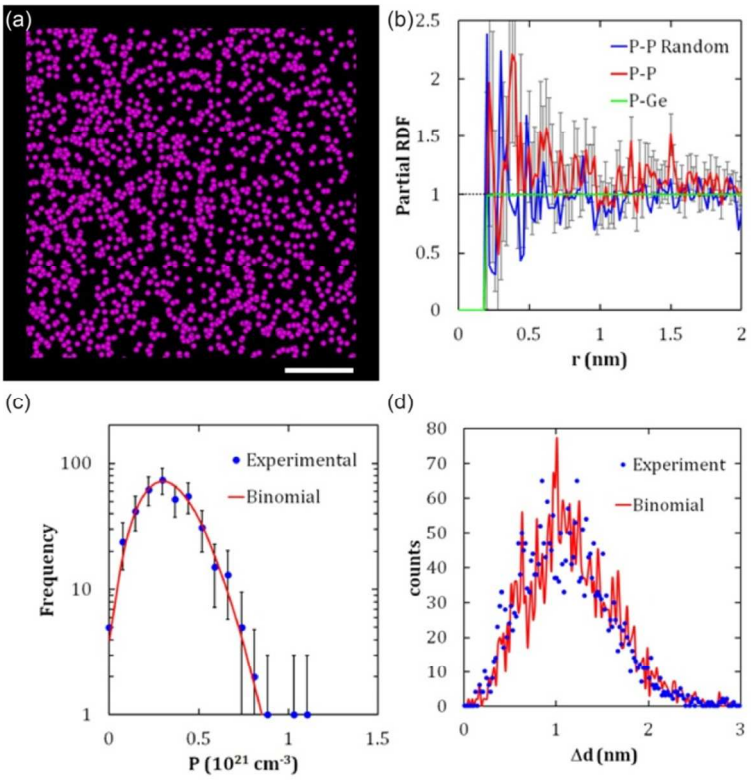

Figure S1. (a) Distribution of Phosphorous dopants in the δ-layers viewed normal to the growth direction. Scale bar = 5nm. (b) Partial radial distribution functions (RDF) analyzed with respect to P ions within the δ-layers. The RDFs were calculated using 0.02nm thick shells and the error bars represent ±2σ for P-P, the red line. The blue solid line was generated by randomizing the atomic species labels of the reconstructed δ-layers and therefore represents a random alloy with the same composition and ion positions of the original. (c) Concentration frequency distribution of P within the δ-layers analyzed in blocks of 600 atoms, with error bars representing ±2σ. This frequency distribution is compared with the binomial distribution, solid line, expected for a random alloy consisting of the same composition. (d) Distribution of the nearest neighbor distances of Phosphorous dopants present within the δ-layers. The solid line corresponds to the binomial distribution expected for a random alloy.

To conclude the Atom Probe Tomography analysis, we report in Figure S2 the isoconcentration surfaces enclosing regions of increasing P concentration. It is found that the doped region horizontally spans the layer as a connected whole up to at least half the maximum P volume density, $< 4\times10^{20}$ P cm^{-3}, and at volume densities approaching the maximum P volume density for the layer form several large isolated volumes and as the concentration increases the lateral extent of the enclosed regions shrinks.

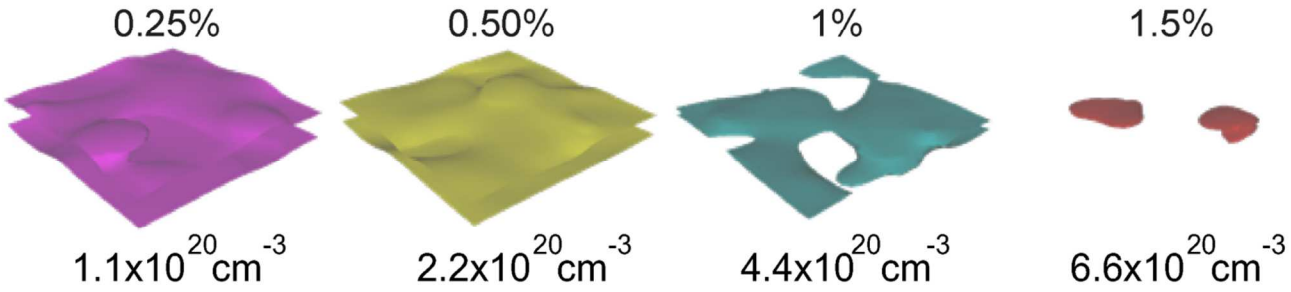

Figure S2. Isoconcentration surfaces with increasing P concentration, shown in both atomic % and the equivalent volume density, for a 30×30×10nm^3 isolated volume containing a δ-doped P layer.

2. Magnetotransport characterization and data analysis

Hall bars structures to investigate the electrical properties of the doped layers were defined by a CHF_3/CF_4 based dry etch with thermally evaporated Al Ohmic contacts. Four-probe magnetotransport characterization was performed using standard low frequency lock-in techniques and low injection currents (~1nA) to measure simultaneously the perpendicular magnetic field B dependence of the longitudinal ρ_{xx} and transverse ρ_{xy} components of the resistivity tensor, where x and y are, respectively, the directions parallel or perpendicular to the current flow in the Hall Bar. The longitudinal σ_{xx} and transverse σ_{xy} (Hall) conductivity were calculated from the measured resistivities via tensor inversion:

$$\sigma_{xx} = \frac{\rho_{xx}}{\rho_{xx}^2 + \rho_{xy}^2}, \qquad \sigma_{xy} = \frac{\rho_{xy}}{\rho_{xx}^2 + \rho_{xy}^2} \qquad (1)$$

Preliminary characterization of the samples was performed at 4 K using a dipstick in liquid helium and magnetic field up to 1 T. Since quantum corrections to the conductivity arising from electron-electron interactions (EEI) and weak localization (WL) at 4K are less pronounced than at lower temperatures, this preliminary characterization allows for a first estimate of the electrically active carrier density $n^0 \sim n(4\text{K})$ and of the Drude

conductivity $\sigma_D \sim \sigma_{xx}(4\text{ K}, 0\text{ T})$, where n(4K) is obtained by fitting the measured transverse magnetoresistance to the Hall relationship $\rho_{xy} = 1/neB$ and $\sigma_{xx}(4\text{ K}, 0\text{ T}) \sim 1/\rho_{xx}(4\text{ K}, 0\text{ T})$, where ρ_{xx}(4 K, 0 T) is the zero field longitudinal resistivity. For measurements at temperatures down to 200 mK the samples were cooled in a dilution refrigerator equipped with a superconducting magnet providing perpendicular fields up to 8 Tesla. Additional measurements between 1.5 K and 10 K were taken in a variable temperature insert with a limited field of up to 0.5 T.

For each sample we separated WL and EEI corrections to the conductivity by analyzing the magnetoresistivity tensor at low temperatures to determine self-consistently the Drude conductivity σ_D and the electrically active carrier density n^0. We started by using n(4K) and $\sigma_{xx}(4\text{ K}, 0\text{ T})$ as approximate values for the classical n^0 and σ_D, then we analyzed the data applying the following procedure:

(i) we eliminated the EEI corrections in the resistivity tensor by estimating the interaction parameter K_{ee} that yielded an optimum fit of the $\rho_{xy}(B)$ curves at all T to the same Hall slope; as a result, a refined estimate of the electron density n^0 was obtained by averaging over the values obtained at all T, from which followed temperature independent estimates for electron scattering time τ_e and diffusion coefficient D;

(ii) using the phase coherent time $\tau_\varphi(T)$ and the pre-factor α as fitting parameters and with τ_e and *D held fixed*, we fit the magnetoconductivity curves $\sigma_{xx}(B) - \sigma_{xx}(0)$ at all T with the Hikami formula[2] $\delta\sigma_{wl} = \alpha G_0 \left[\Psi\left(\frac{1}{2} + \frac{B_\varphi}{B}\right) - \Psi\left(\frac{1}{2} + \frac{B_0}{B}\right) + \ln\frac{B_0}{B_\varphi}\right]$ (2) that describes the WL correction to the conductivity, where $G_0 = e^2/\pi h$, and B_φ and B_0 are the characteristic phase and transport relaxation fields related to τ_φ and τ_e by $B_\varphi = \hbar/4De\,\tau_\varphi$, and $B_0 = \hbar/4De\,\tau_e$. Note that the transport relaxation field B_0 sets the range of validity of the Hikami formula ($B \ll B_0$) and represents the magnetic fields above which WL corrections are suppressed. Owing to the short τ_e typical of Ge:P 2DEGs (~10^{-14} s), B_0 ranges from ~1 to ~5 Tesla, making the Hikami fit applicable over a relatively large magnetic field range compared to higher mobility 2DEGs obtained in GaAs[3] or Si/SiGe[4] based 2DEGs.

(iii) subsequently, σ_D was estimated at all T using the equation $\sigma_{xx}(0) = \sigma_D + \alpha G_0 ln\left[\frac{\tau_e}{\tau_\varphi(T)}\right] + K_{ee} G_0 ln\left(\frac{kT\tau_e}{\hbar}\right)$ (3), which describes for the longitudinal conductivity of a disordered 2DEG at low temperatures and zero magnetic field;

(iv) finally a refined estimate of σ_D was obtained by averaging over the values at all T.

The obtained estimates of σ_D and n^0 were then used as starting parameters in the self-consistent iterations. The self-consisting procedure described in steps (i)-(iv) was iterated until convergence is reached with a standard deviations on the temperature-averaged n and σ_D of less than 1%.

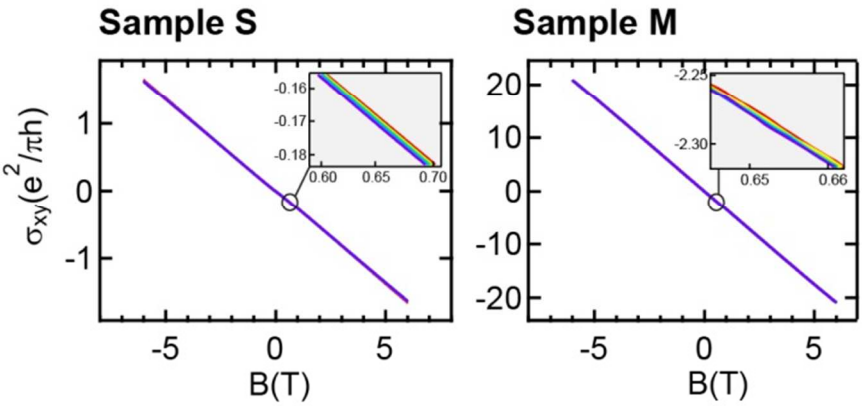

Figure S3. Original transverse $\sigma_{xy}(B)$ magnetoconductance curves with inset highlighting temperature independence. Measurement temperatures for sample S: 0.3 K (purple), 0.5 K (blue), 0.7 K (green), 0.9 K (yellow), 5 K (red); sample M: 0.2 K (purple), 0.35 K (blue), 0.5 K (cyan), 0.7 K (green), 0.9 K (yellow), 5 K (red).

To have further insights into the magnetotransport measurements and data analysis, we report in Figure S3 the $\sigma_{xy}(B)$ curves obtained directly by tensor inversion of the experimental curves $\rho_{xx}(B)$ and $\rho_{xy}(B)$ at different temperatures. For both samples investigated, all $\sigma_{xy}(B)$ curves at different temperatures lie on top of each other over the entire magnetic field range. This temperature *independence* of σ_{xy} is in agreement with EEI theory of disordered 2DEGs[5] that predicts corrections to σ_{xx} only. It confirms also that mobility μ, n^0, and thus σ_D, are constant over the entire temperature range investigated,[6] therefore validating the theoretical framework and data analysis procedure used in this *Letter*.

To conclude the magnetotransport analysis, in Figure S4 we report the magnetic field dependence of the ratio $\sigma_{xy}^2/\sigma_{xx}^2$ at high (5 K) and low (0.3K) temperatures for samples S (solid lines) and M (dashed lines), respectively. We find that $\sigma_{xy}^2/\sigma_{xx}^2$ is small (< 0.01) throughout the whole magnetic field investigated, because of the

relatively low mobility in these samples caused by scattering from ionized impurities in the δ-layer planes. This validates the use of Eq. 3 to evaluate the corrections to the measure the Hall coefficient, as explained in Ref. (7).

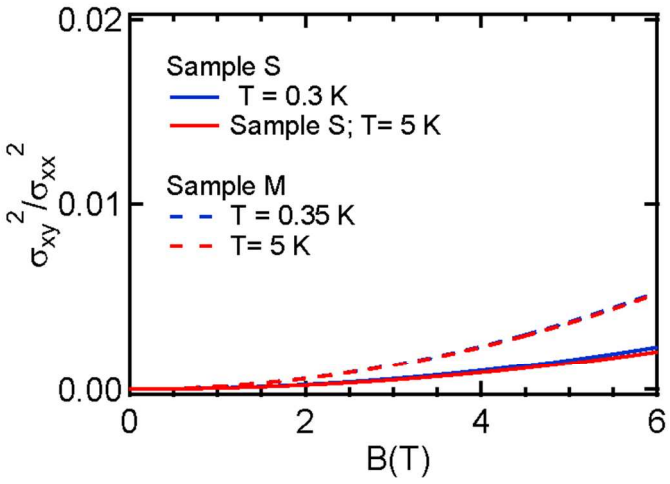

Figure S4. Squared ratio between transverse and longitudinal conductance as a function of magnetic field for sample S (solid lines) and sample M (dashed lines). Measurement temperatures for sample S: 0.3 K (blue), 5 K (red); sample M 0.35 K 5 K (red).

References

(1) Riley, J.R.; Perea, D.E.; He, L.; Tsui, F.; Lauhon, L.J. *J. Phys. Chem. C* **2012**, 116, 276.

(2) Hikami, S.; Larkin, A. I.; Nagaoka, Y. *Prog Theor Phys* **1980,** *63*, 707.

(3) McPhail, S.; Yasin, C. E.; Hamilton, A. R.; Simmons, M. Y.; Linfield, E. H.; Pepper, M.; Ritchie, D. A. *Phys Rev B* **2004,** *70* 245311.

(4) Scappucci, G.; Di Gaspare, L.; Evangelisti, F.; Giovine, E.; Notargiacomo, A.; Leoni, R.; Piazza, V.; Pingue, P.; Beltram, F. *Phys Rev B* **2005,** *71* 245311.

(5) Altshuler, B. L.; Aronov, A. G.; Lee, P. A. *Phys Rev Lett* **1980,** *44*, 1288.

(6) Jouault, B.; Jabakhanji, B.; Camara, N.; Desrat, W.; Consejo, C.; Camassel, J. *Phys Rev B* **2011,** *83*, 195417.

(7) Goh, K. E. J.; Simmons, M. Y.; Hamilton, A. R. *Phys Rev B* **2007,** *76*, 193305